JOURNAL OF MATERIALS SCIENCE 26 (1991) 5655–5663

On the growth mechanism of silicon carbide whiskers

G. McMAHON
Ceramics Kingston Inc., Kingston, Ontario, Canada
G. J. C. CARPENTER, T. F. MALIS
Metals Technology Laboratory, CANMET, Ottawa, Ontario, Canada

The microstructure of SiC whiskers has been studied through analytical electron microscopy. The whiskers were found to contain discrete regions of high and low planar defect density. These regions of low defect density were identified as 3C beta-SiC, whereas the regions of high defect density were consistent with a mixture of SiC polytypes, with the 3C and the 6H polytypes being the most predominant as a result of the formation of a high density of microtwins on the (1 1 1) planes perpendicular to the ⟨1 1 1⟩ growth direction. A growth mechanism is suggested based on observations of (a) outer layers of SiC on vapour–liquid–solid catalysts and (b) C:Si variations between the regions of high and low densities of planar defects. It appears that there is some degree of stoichiometric control over the microstructure of the SiC whiskers in that slight carbon enrichments seem to promote the growth of relatively defect-free regions of beta-SiC whiskers.

1. Introduction

The potential of advanced ceramic materials for high-temperature applications has generated considerable interest. Among these applications are advanced heat engines, where there is an incentive to produce light-weight structural materials with high-temperature performance capabilities superior to cobalt- and nickel-based superalloys. However, one of the factors which has inhibited the use of ceramic materials is a high sensitivity to processing and service-generated flaws, which is ultimately reflected in the low fracture toughness values typical of monolithic ceramic materials.

In order to reinforce and toughen ceramic materials, fibres or whiskers have been added to ceramic matrices, producing an improved fracture toughness [1–3]. Due to their high-temperature strength and chemical stability, SiC whiskers have received considerable attention.

1.1. Structure of silicon carbide

Before considering growth mechanisms for SiC whiskers, it is first necessary to understand the complex crystallography of this material. This complexity arises from the ability of SiC to crystallize into many different structural types, commonly called polytypes. The phenomenon of polytypism stems from the capacity of a solid to crystallize into more than one modification having essentially the same chemical composition, but differing in the number and the manner of stacking of layers in the unit cell.

The stacking sequence of SiC may be represented by a close-packing of spheres, and any structure can be represented by specifying the stacking order of the close-packed planes on three possible stacking positions, A, B and C. Since SiC has a double layer, one close-packed layer specified in terms of packing of spheres actually represents two combined layers, a carbon layer and a silicon layer. For example, the basic stacking sequence of cubic SiC is shown in Fig. 1. If the first layer is denoted as stacking position A, the second close-packed layer, which can then be placed at either stacking position B or C, is placed at stacking position B. Similarly, the third layer is located at position C, producing a stacking sequence of ABCABC . . . , as indicated by the solid line in Fig. 1. Stacking sequences which repeat on a different basis produce other polytype structures. The notation to describe polytype structures follows that first suggested by Ramsdell [4]. In this notation, a number is

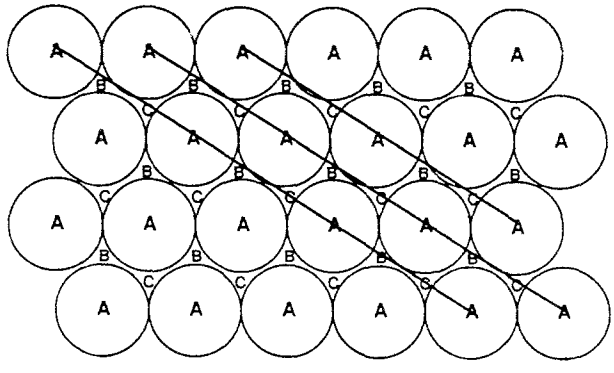

Figure 1 Stacking positions for SiC showing stacking sequence of 3C beta-SiC as represented by a close-packing of spheres.

0022–2461/91 $03.00 + .12

assigned corresponding to the number of layers in the unit cell, combined with a letter designating the crystal symmetry (C representing cubic, H hexagonal and R rhombohedral). The most common polytypes found are the alpha 6H (stacking sequence ABCACB), 4H (ABCB) and the beta 3C (ABC) modifications. However, many polytype structures with larger unit cells have also been found and are summarized elsewhere [5, 6].

The low stacking-fault energy of SiC (1.9 erg cm^{-2} or 1.9×10^{-3} J m^{-2} [7]) implies that fault or twin interfaces add relatively little to the free energy of the structure and hence, under appropriate growth conditions, several close-packed structures could be energetically feasible. Thus, mixed polytypes and frequent faults or microtwins within polytypes may occur, and when the twin or fault frequency is great and the distance between them irregular, the structure is said to be one-dimensionally disordered. Shinozaki and Kinsman [8] have ascribed a necessary condition for the one-dimensional disordered structure in SiC as the intergrowth of faulted cubic 3C beta-SiC regions among thin regions of hexagonal alpha-SiC polytypes. For example, if the stacking sequence in an SiC crystal is found to be . . . ABCBABCACBABCABC . . . , no apparent regular stacking sequence is observed, and so this structure would represent one-dimensionally disordered SiC. By breaking this stacking sequence down into its component polytypes, . . . ABCB/ABCACB/ABCABC . . . , it is observed that this stacking sequence is actually comprised of one unit cell of the hexagonal 4H and 6H alpha-SiC polytypes and two unit cells of the 3C beta-SiC polytype. Thus, one-dimensionally disordered SiC can arise from the intergrowth of short-period alpha and beta SiC polytypes.

1.2. Growth of silicon carbide whiskers

Whiskers of silicon carbide have been produced by a number of methods, most of which may be categorized by a vapour–liquid–solid (VLS) growth mechanism. The VLS mechanism was first proposed by Wagner and Ellis [9] for the growth of silicon whiskers. Since that time, a number of workers have produced evidence that the VLS growth mechanism may also be applied to silicon carbide [10–16].

The VLS growth mechanism differs from the more conventional liquid–solid and vapour–solid crystal growth theories in that a layer of liquid in which the crystal material itself (or its components) is soluble is situated between the vapour and the growing crystal. The surface of the liquid is a preferred site for deposition from the vapour phase, and so once the liquid becomes supersaturated with the reacting species, crystal growth occurs by precipitation at the solid–liquid interface. This mechanism is well documented for the growth of silicon whiskers [9]. However, the VLS growth mechanism of silicon carbide whiskers, and its effect on the resultant crystal structure, is not well understood. It is the object of this paper to address this particular problem.

2. Experimental procedure

The SiC whiskers studied were obtained through a proprietary process developed by Ceramics Kingston Inc. The material was prepared for analytical electron microscopy (AEM) examination by dispersing the whiskers on to copper grids with and without carbon support films. For cross-sectional examination, the whiskers were embedded in both Epon and Spurrs epoxy, sectioned with a Reichert-Jung ultramicrotome at set thicknesses of 40–80 nm and collected on copper grids. A stroke rate of 0.1 mm s^{-1} gave the best results, although rates up to 3.0 mm s^{-1} were tried. The microtomed sections were then dispersed on to copper grids with and without carbon support films. All specimens were examined in a Philips EM400T transmission electron microscope (TEM) equipped with an EDAX 9100/60 energy-dispersive X-ray analysis system (EDS) and a Gatan 607 instrument for serial electron energy loss spectroscopy (EELS). All TEM investigations were performed using a lanthanum hexaboride source.

2.1. Electron energy loss spectroscopy

Two different methodologies were used to determine C:Si ratios through EELS analysis. In both methods, the specimens examined were those on copper grids without carbon support films. The spectral collection methods are detailed elsewhere [17] but may be summarized as follows.

Method 1 involved collection of the low energy Si*L* core loss edge (90 eV) and the C*K* edge (284 eV) at 1 eV per channel and a 29 mrad collection angle (2 mm spectrometer entrance aperture and a 34 mm camera length) in diffraction pattern-on-screen mode using a 30–50 nm, high-intensity nanoprobe beam. These edges both have high signal/noise ratios, but the signal/background ratio for the Si*L* edge is low for all but very thin specimens. Drift effects are minimized by a relatively short serial EELS collection time.

Method 2 involved collection of the C*K* edge and the high-energy Si*K* core loss edge (1840 eV) at 2 eV per channel, with other settings as in Method 1. Although the signal/noise ratio for the Si*K* edge is poor and collection times are increased by a factor of ten, the greater ease and reproducibility of background fitting for both edges ultimately made this method more reproducible for the typical whisker diameters studied. Measures taken to minimize drift effects included choosing physically stable whiskers (under the electron beam), periodically stopping the collection to view the beam position, and comparing spectra obtained from low to high energy loss and the reverse. The latter tests showed no significant changes in the C:Si ratios, nor were there any different trends in C:Si ratios when comparing analyses for the few whiskers thin enough for Method 1 analysis with the majority of the thicker whiskers. The experimental or calculated partial cross-sections used for quantification by both methods were judged to have similar accuracies [17, 18]. In both methods, an integration window of 100 eV was used for the quantification.

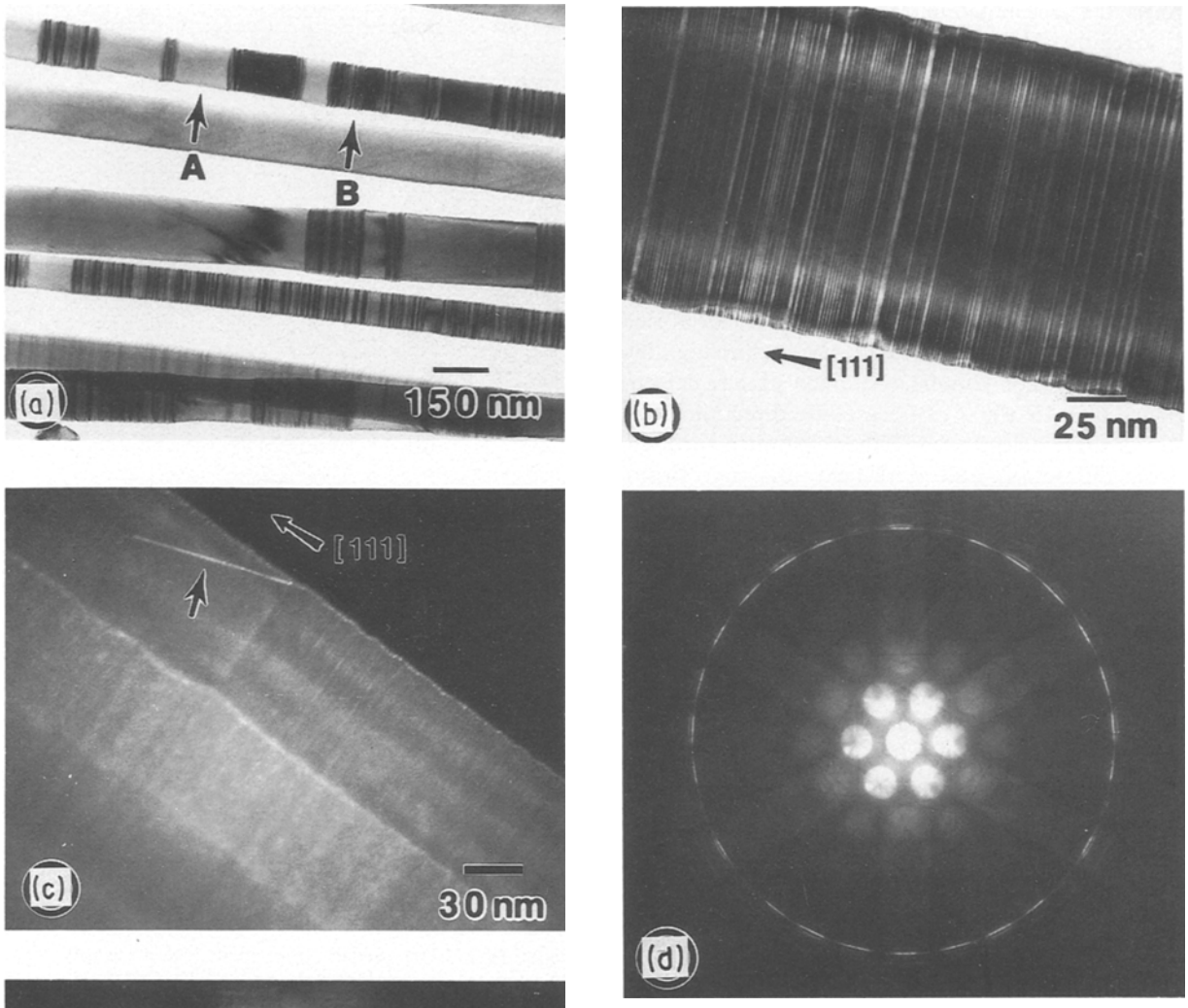

Figure 2 (a) Bright-field overview of SiC whiskers, with regions typical of those used for EELS analysis labelled A and B; (b) bright-field image of high planar defect density region viewed along ⟨1 1 0⟩ zone axis; (c) dark-field image showing microtwin in low defect density region; (d) ⟨1 1 1⟩ CBED pattern from low defect density region; and (e) HOLZ line pattern from (d).

3. Observations

A general overview of the dispersed whiskers is shown in Fig. 2a. The diameter of the whiskers was typically between 75 and 175 nm; however, whiskers with diameters as low as 50 nm and as large as 750 nm were occasionally observed. Most of the whiskers studied contained discrete regions differing greatly in planar defect density and possessing slightly different diameters, as can be seen in Fig. 2a. A magnified view of a high defect density region is shown in Fig. 2b, where the whisker was oriented such that a ⟨1 1 0⟩ zone axis was accurately parallel to the electron beam. The high density and irregular spacing of the planar defects is readily observed under strong, many-beam imaging conditions. The faults observed in regions such as this were oriented parallel to the {1 1 1} planes perpendicular to the growth direction. By carefully orienting whiskers in this manner and imaging in diffraction contrast, it was possible to conclude that fault spacings as small as a few atom planes were present in such regions.

These regions of high planar defect density were often found to be linked via another planar defect along other {1 1 1} planes at an angle of 70.5° to the growth plane. By imaging in dark-field using a reflection which would correspond to a twin reflection along this {1 1 1} plane, as in Fig. 2c, it was concluded that these planar defects were also microtwins. Statistical analysis of a number of whiskers showed that the proportion of high and low defect density regions was approximately equal. The structure of the low defect density regions was confirmed through electron diffraction to be cubic beta-SiC. Fig. 2d and e show ⟨1 1 1⟩ convergent-beam electron diffraction (CBED)

patterns taken using different camera lengths from such a region. The reciprocal lattice spacing experimentally determined using the high-order Laue zone (HOLZ) ring diameter in Fig. 2d agrees with the calculated result for cubic beta-SiC. The threefold symmetry clearly evident in the HOLZ lines of Fig. 2e confirms the face-centred cubic structure.

The structure of the regions containing a high density of planar defects was, however, much more complex. The ease with which stacking faults may be incorporated into the structure of SiC has been described in section 1.1, and it is thus not surprising that half of the whisker volume contained planar defects perpendicular to the $\langle 1\,1\,1 \rangle$ growth direction. The nature of these defects was further examined through electron diffraction and dark-field imaging. From these investigations, it was observed that many of the defect-free regions were in twin orientations with each other. A dark-field image of a whisker segment and an accompanying selected-area diffraction pattern (SADP) from the region indicated are shown in Fig. 3a and b, respectively. The SADP observed clearly shows a second set of reflections which are well known to be twin reflections [19]. The dark-field image in Fig. 3a was taken using a twin reflection, and shows seven low defect density regions varying from approximately 3 to 250 nm in length and in varying twin relations to one another and the high defect density regions.

In Fig. 4, an SADP from a region containing a high density of planar defects is shown. Although the main intensity maxima may be indexed as 3C beta-SiC, the streaking observed along the reciprocal lattice rows

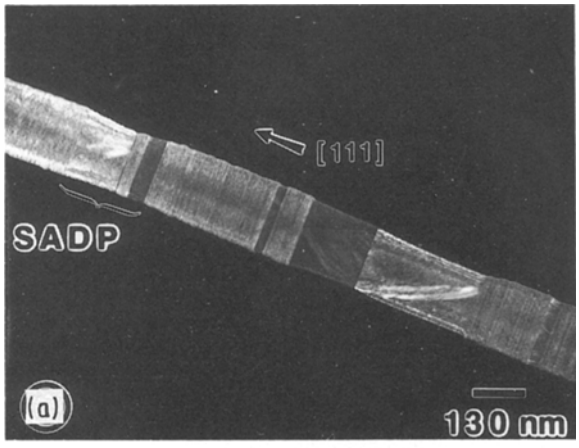

Figure 3 (a) Dark-field image of whisker segment showing high and low defect density regions of varying length in twin relations; (b) $\langle 1\,1\,0 \rangle$ SADP from region labelled in (a).

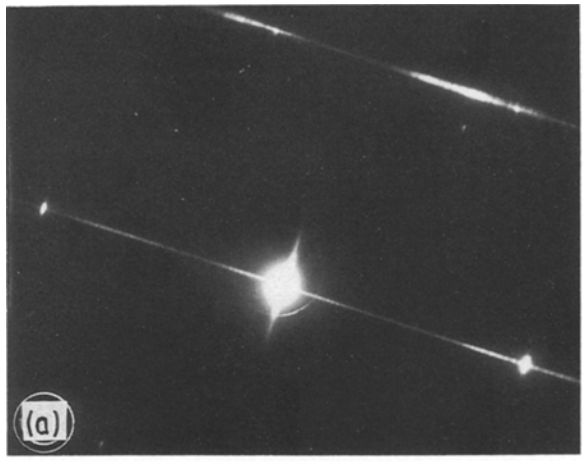

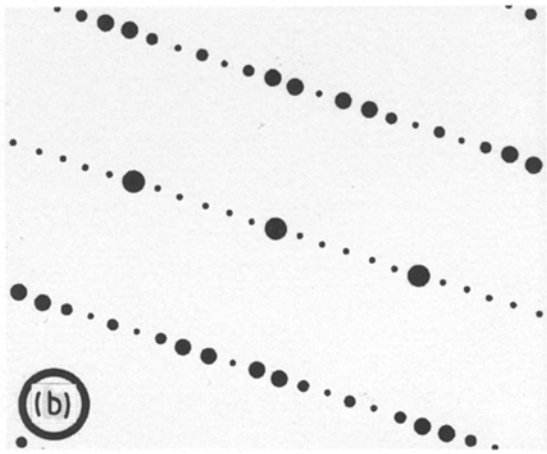

Figure 4 (a) $\langle 1\,1\,0 \rangle$ SADP from high defect density region; (b) computer-simulated 6H alpha-SiC $\langle 1\,1\,\bar{2}\,0 \rangle$ SADP showing similar maxima along systematic rows.

indicates a high density of either stacking faults, microtwins or a combination of the two. The fact that strong alternating diffraction contrast is observed in dark-field images using twin reflections indicates that the majority of these planar defects were microtwins, consistent with earlier observations [20–27].

Cross-sectional examination of microtomed sections revealed the whiskers to be in the shape of rounded triangles, an example of which is shown in Fig. 5. These cross-sections frequently contained complex arrays of fault-like defects, as seen in Fig. 5, which is believed to be a section through a low defect density region of a whisker. Bright field/dark field comparisons of edge fringes for isolated defects in the microtomed cross-sections confirmed that at least some of them showed contrast changes suggestive of stacking faults. However, defects formed by the impact/cleavage process of diamond knife sectioning may not be ruled out, although relatively defect-free cross-sections were observed as well. (As an aside related to ultramicrotomy for microanalysis/elemental mapping, the thicknesses of several sections were measured with EELS using the method described by Malis *et al.* [28]. Significant variations were found in many cases even with such small whisker diameters. This is likely to be a result of the whisker cleavage plane not being parallel to the sectioning plane, producing a wedge-shaped section.)

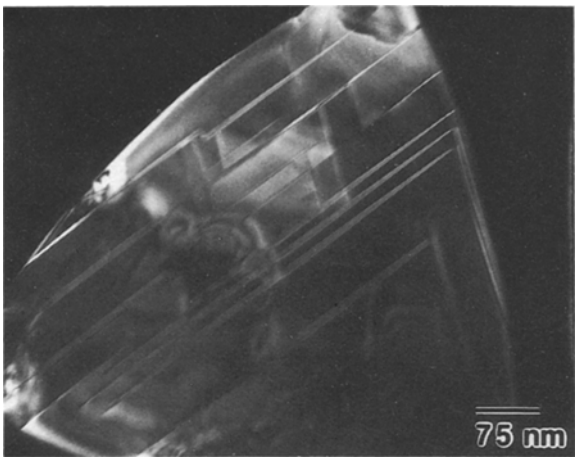

Figure 5 Dark-field image of a typical SiC whisker cross-section.

Some of the whiskers showed globules at their tips, consistent with a VLS-related crystal growth mechanism. Examples of such a VLS crystal growth catalyst are shown in Fig. 6. EDS analysis indicated that the bulk of the catalyst was iron- and silicon-enriched. A common observation for all VLS catalysts was the presence of a defective crystalline outer layer of varying thickness surrounding the bulk of the catalyst. A typical example of such a layer is observed in Fig. 6a, and a more extreme case of a very thick layer is observed in Fig. 6b. The presence of a Si peak in the EDS spectra and a C*K* edge in the EELS spectra from these regions suggested that this outer layer might be SiC. This postulate was confirmed through electron diffraction. These catalyst surface layers were found to be typically 25–100 nm in thickness, crystalline in nature, and exhibiting an alternating defect structure similar to the whisker itself, that is, a non-periodic distribution of regions of abrupt variations in defect density.

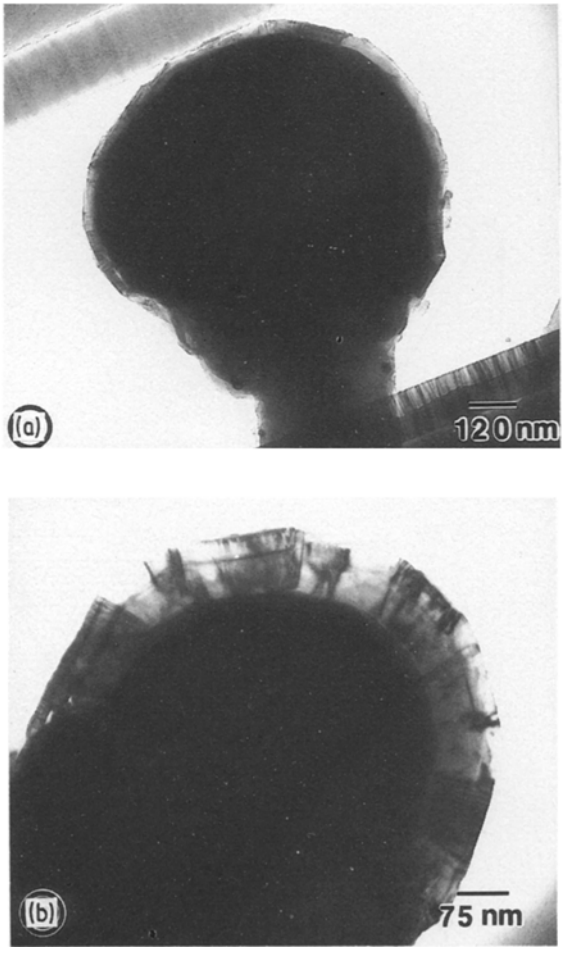

Figure 6 (a) Bright-field image showing typical SiC layer surrounding VLS catalyst; (b) extreme case of very thick layer.

Electron energy loss analysis of the whiskers was conducted at various locations along the length of the dispersed whiskers, as exemplified by the regions labelled A and B in Fig. 2a. Initial results indicated a consistent difference of the C:Si ratios across the interfaces between regions of low and high defect density and little difference within these regions. The results suggested that the low defect density regions had associated with them a higher C:Si ratio than the regions with a high density of defects. Further analyses concentrating on these interfaces were conducted in two ways; a few analysis pairs across interfaces in a large number of whiskers, followed by more detailed traces along a smaller number of whiskers. While the great majority of individual interfaces showed a higher C:Si in the low defect density region, more relevant statistics could be determined for the single whisker traces. Two such traces gave mean values of C:Si (low defect density) to C:Si (high defect density) of 1.11 ± 0.09 and 1.08 ± 0.07. Since the errors represent 95% confidence levels, we are led to believe that the low defect density regions indeed have a higher C:Si ratio.

4. Discussion

4.1. Electron diffraction analysis

It is well known that stacking faults (including twin boundaries) can give rise to streaking in the diffraction patterns along the direction perpendicular to the fault planes [29]. Carter [30] has shown that a series of closely spaced faults leads to the intensity maxima along the streaks, having a spacing in a reciprocal relationship to the repeat distance of the faults. For example, in the case of a series of microtwins having a constant thickness of 10 atom planes, the streaks along the 1 1 1 systematic row of reflections would be divided into 10 intensity maxima. In practice, we have a distribution of twin spacings (typically 0.2–2.5 nm in thickness), which gives rise to a multitude of closely spaced maxima as observed in Fig. 4. Computer simulation was carried out for a 6H alpha-SiC diffraction pattern for a $\langle 1\,1\,\bar{2}\,0 \rangle$ zone axis. Similar diffraction maxima along the 1 1 1 systematic rows were obtained, as shown in Fig. 4b. This is a result of the 6H polytype being equivalent to a twinned 3C polytype. As the repeat distance in a polytype increases, the effect on the simulated diffraction patterns is a smearing out of the intensity maxima along the reciprocal lattice rows. Thus, essentially the same result is obtained from a consideration of the effect of multiple twinning on the diffraction patterns. It therefore appears that the occurrence of polytypes may simply be a consequence of the presence of a high density of microtwins in the SiC whiskers.

4.2. Electron energy loss analysis

The EELS results indicated that there was an increased C:Si ratio associated with the low defect density regions of the whiskers. The significance of this composition difference is enhanced by the fact that it is a relative quantitative comparison, hence many of the inaccuracies inherent in absolute EELS quantification (cross-sections, background subtraction, plural scattering differences) are either minimized or eliminated. However, the absolute values of the C:Si ratios in both regions were always higher than the expected stoichiometric value of 1.0, and varied from whisker to whisker, ranging from 1.10 to 1.45.

It is postulated that the reason for this apparent carbon enrichment is a combination of direct vapour deposition of carbon on the whisker during the growth process, and/or the normal carbon contamination associated with TEM studies. An example of evidence for such coatings is shown in Fig. 7, where bright field/dark field comparisons clearly indicate the presence of a coating approximately 10 nm in thickness. The contrast of this coating in the dark-field image suggested that it is amorphous in nature. Further studies combining EELS analysis, microdiffraction and conical dark-field imaging suggested that it was most likely to be amorphous carbon, and not SiO_2 or a silicon oxycarbide, as the presence of oxygen was not detected in EELS spectra from these layers.

The effect of a small carbon coating on the whisker surface in the EELS results can be explained with the aid of Fig. 8. If a cross-section of a typical whisker is represented as an equilateral triangle with sides 100 nm in length (Fig. 8a), then the total volume of the whisker interacting with the electron beam (assuming 100 nm spot size and 100 nm specimen thickness) may be found through geometric calculations. Since the volume and the number of Si and C atoms in the SiC unit cell are known, the number of both Si and C atoms may be estimated as

$$\text{Number Si atoms} = 2.10 \times 10^7$$

$$\text{Number C atoms} = 2.10 \times 10^7$$

If a 10 nm carbon layer is formed on the surface (e.g. Fig. 8b), then the new volume (now assuming 120 nm specimen thickness and 100 nm spot size) under the electron beam may be calculated. The volume of the C layer may then be found by subtraction and if the C layer is assumed to be graphite, the number of C atoms in this layer may be roughly estimated (since the C layer actually appears to be amorphous) as

$$\text{Number C atoms in layer} = 9.38 \times 10^6$$

Therefore, the C:Si ratio in this case would be

$$\text{C:Si} = (9.38 \times 10^6) + (2.10 \times 10^7)/(2.10 \times 10^7)$$

$$= 1.45$$

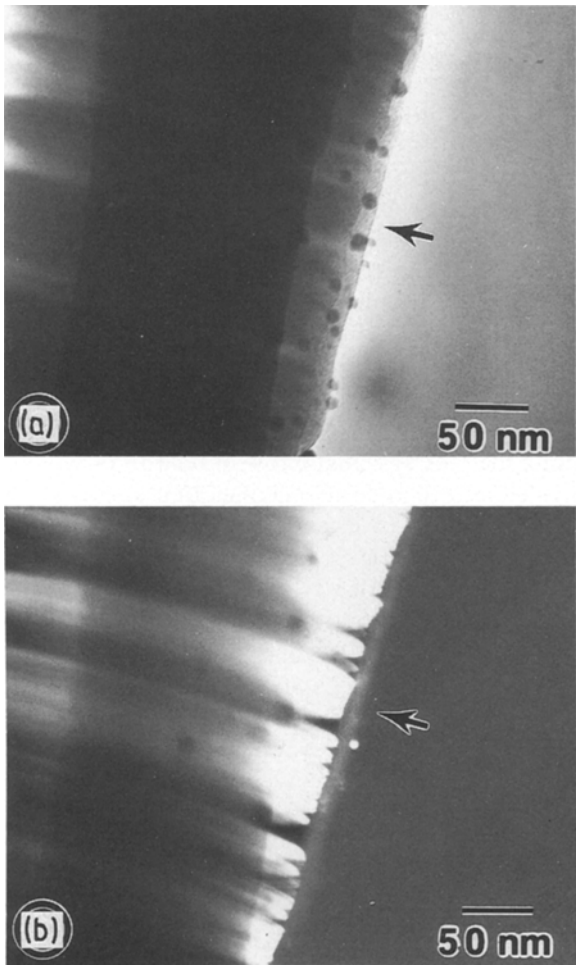

Figure 7 (a) Bright-field image showing amorphous carbon coating on whisker surface; (b) dark-field image of (a) using SiC reflection.

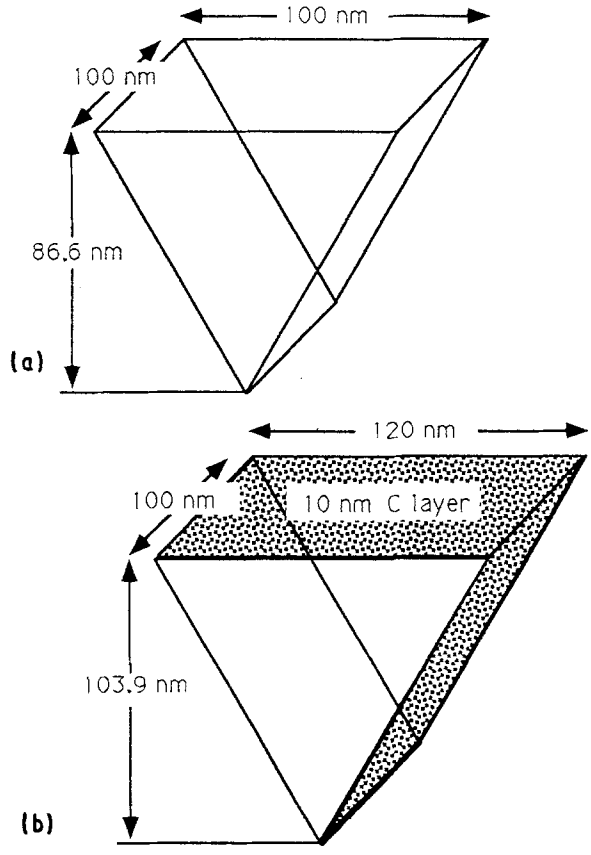

Figure 8 Schematic representations of SiC whisker segment (a) without and (b) with a 10 nm surface layer of carbon.

Hence, small surface layers of pure C or enriched in C can effect the C:Si ratios obtained through EELS analysis significantly. To further test this hypothesis, C:Si ratios were determined on the microtomed cross-sections in order to alleviate the effect of C-enriched surface layers. Although it was difficult to determine whether a certain cross-section constituted a high or low defect density region, the values obtained (0.98–1.04) are indicative of stoichiometric SiC, and were independent of the sampling location within the whisker cross-section.

The existence of some form of carbon-rich layer is significant in that it may affect the mechanical performance of whisker-reinforced composites. It has recently been shown [31] that changes in the surface chemistry of SiC can have a considerable effect on the fracture toughness of a ceramic-matrix composite. The extent to which the stoichiometric discrepancies and structural changes in the bulk of the whisker affect the mechanical properties of both metal and ceramic matrix composites is still unknown, but the existence of such structural and chemical changes in not only these but possibly other SiC whiskers should be borne in mind when interpreting interfacial phenomena in composite materials.

In the past, the question of the effect of stoichiometry on the structure of SiC has only been lightly addressed, and the results are in poor agreement. The effect observed in this study may be similar to that which led Ryan *et al.* [11] to postulate that the reason for obtaining hexagonal alpha-SiC whiskers at low temperatures might be associated with slight carbon deficiencies as compared to the stoichiometry of cubic beta-SiC whiskers. As the regions of high defect density in the present study were thought to consist of an intergrowth of a small amount of alpha in a predominantly beta-SiC structure (similar to that described by Jepps and Page [32]), these results would lend some support to the theory of Ryan *et al.* [11]. Other workers, however [33–36], have observed the opposite effect, concluding that increasing the C:Si ratio led to an increasingly hexagonal structure, with the change in the C:Si ratio affecting primarily the nucleation of a given polytype. While contradictory regarding which structure is favoured, all of this work is consistent with a model suggesting that changes in the C:Si ratio in the VLS growth catalyst dictate whether a whisker portion grows with a pure cubic structure or a structure with a high density of planar defects or mixed polytypes.

An alternative explanation of the C:Si discrepancies may lie within the possible existence of inversion twins, in which both a polarity reversal of the SiC unit tetrahedron and a twinning orientation change is observed to occur at the twin boundary. Therefore, two types of inversion twins may occur, a positive type and a negative type, in which the charges of the atoms lying adjacent to the mirror plane leave an excess of positive or negative charges at the twin boundary [37]. As we have observed a decrease in the C:Si ratio in the regions of high defect density, it is possible that this discrepancy is a result of the formation of a high density of positive inversion twins, producing a higher local distribution of Si atoms and hence positive charge at the twin boundary.

As the solubility of Si in the Fe-enriched VLS catalyst is much higher than that of carbon, the occurrence of such twins during the growth process may not be so unreasonable. Austerman and Gehman [37] have inferred the existence of inversion twins in many compounds with sphalerite-type crystal structures, including SiC. Some support for this theory was given in a recent study on the growth of chemical vapour-deposited beta-SiC in which the density of antiphase boundaries (of which the inversion twin is a special case) diminishes with increasing C:Si ratios in the reactant gases. It was further suggested that these antiphase boundaries originate in Si–Si bonds, rather than at C–C bonds [38]. However, studies on ZnSe (also of the sphalerite structure) have shown that great care in lattice imaging and computer simulation of lattice images is required to confirm the existence of inversion twin boundaries [39].

4.3. VLS growth mechanism

It is not surprising that the VLS growth catalysts observed in this study were Fe- and Si-enriched as iron has long been known to be an effective catalyst for VLS whisker growth [11, 13–15, 40, 41]. However, the observation and structure of the outer layer of the VLS catalyst now gives some support for the VLS growth model for SiC proposed by Shchetanov *et al.* [42] and the formation of the bamboo-type structure which they frequently observed in SiC whiskers. A brief explanation of the initial part of their mechanism may be given with the aid of Fig. 9. It is based on the assumption that during stable growth via a VLS mechanism, the number of Si and C atoms passing into the liquid phase should be equal to the number passing into the solid phase (Fig. 9a). However, when fluctuations occur in the composition of the gas phase, a concentration sufficient for the generation of SiC may be reached in the surface layers of the liquid VLS catalyst, depending upon their solubility of carbon and silicon. If this is the case, crystallites incoherent with respect to the main crystal may develop, causing a gradual filling of the surface of the drop with SiC and

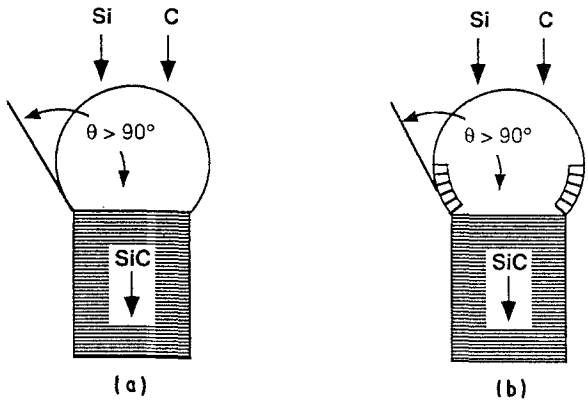

Figure 9 Schematic diagram showing formation of SiC layer around the VLS catalyst: (a) equilibrium growth and (b) formation of outer layers as a result of fluctuations in Si and C concentrations.

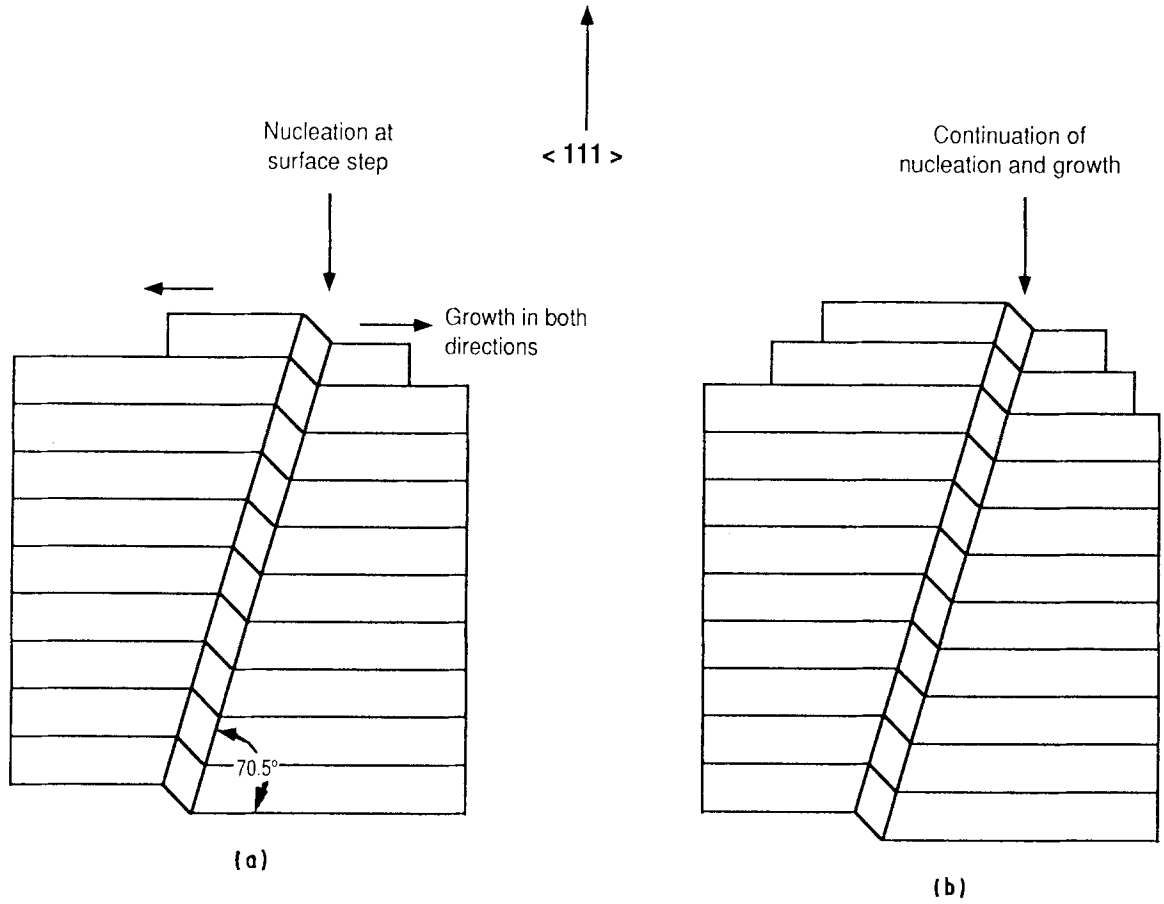

Figure 10 Growth model for low defect density regions: (a) nucleation at surface step formed by microtwin and (b) continuation of nucleation and growth.

the formation of a spherical shell surrounding the VLS catalyst (Fig. 9b). The observations in this study provide direct evidence of the SiC shell surrounding the VLS drops; however, no crystals incoherent with the body of the whisker were ever observed in our studies.

Having established that the VLS catalyst is saturated in Si and C, the next steps in the growth process would be the nucleation and subsequent growth of the SiC whisker. Nuclei of SiC may be formed through a series of reactions within the VLS growth catalyst. Once these nuclei reach a critical radius, crystal growth will be energetically favourable and so the initial stages of growth in a $\langle 1\,1\,1 \rangle$ direction occur. The next nuclei to form may do so on one of two different stacking positions on top of the initial growth. If the "wrong" stacking position is chosen, then a stacking fault or twin boundary occurs. Such processes may repeat themselves, giving rise to the regions of high planar defect (in this case, microtwins) density observed in this study. However, it is possible that nuclei may form oriented along another $\{1\,1\,1\}$ plane at an angle of 70.5° to the growth plane. Nuclei with such an orientation would form steps with nuclei of the previous $\{1\,1\,1\}$ orientation, providing energetically favourable sites for continued growth without a high density of microtwins (shown schematically in Fig. 10a and b). Such a mechanism is consistent with the common occurrence of a thin microtwin in the low defect density regions. These twins ultimately terminate at the whisker edge, such that no further step growth is possible. However, others were found to terminate prematurely, evidently by a mistake in the step growth process. In either case, the nucleation and growth process would then resume. Such a mechanism is, in many respects, similar to the mechanism described by Gleiter [43] for the formation of annealing twins, except in this case atoms are supplied through the VLS catalyst, rather than from an adjacent grain.

5. Conclusions

The microstructure of SiC whiskers produced by Ceramics Kingston Inc. has been studied through AEM. The whiskers were found to contain discrete regions of high and low planar defect density. The regions of low defect density were identified as 3C beta-SiC, whereas the regions of high defect density were consistent with a mixture of SiC polytypes, with the 3C and the 6H polytypes being the most predominant as a result of the formation of microtwins.

Observations of SiC outer layers on VLS catalyst impurities suggest that fluctuations in the composition of the gas phase are occurring. These fluctuations are most likely responsible for the compositional differences observed in the high and low defect density regions of the SiC whiskers. This difference was altered by the presence of a carbon-enriched layer, typically less than 10 nm and non-uniform in thickness, found on most whiskers. Slight enrichments of carbon appear to stabilize a lower energy (lower defect density)

structure, or alternatively, slight carbon depletion encourages frequent growth defects leading to a slightly higher energy (owing to the low stacking fault energy) high defect density structure.

If this hypothesis regarding stoichiometric control of the structure of SiC is valid, then theoretical control of the microstructure of the whisker could be possible, but would appear to be a significant challenge, given the local chaotic conditions anticipated at the vapour–liquid interface and (to a lesser extent) at the solid–liquid interface.

Acknowledgements

The authors would like to thank G. Williams, M. Charest and T. Euser for technical assistance. Valuable discussions with Dr Z. Wronski are also gratefully acknowledged. Financial assistance from the National Research Council of Canada in the form of an Industrial Research Assistance Programme contribution is acknowledged by one of the authors (G.M.). Permission from Ceramics Kingston Inc. to publish this work is greatly appreciated. The contributions of Dr T. A. Wheat, Dr A. K. Kuriakose and Dr A. Ahmad of the Ceramic Section, CANMET and R. T. Holt of NAE/NRC are also gratefully acknowledged.

References

1. Y. AKIMUNE, Y. KATANO and K. MATOBA, *J. Amer. Ceram. Soc.* **72** (1989) 791.
2. L. BJORK and L. A. G. HERMANSSON, *ibid.* **72** (1989) 1436.
3. G. PEZZOTTI, I. TANAKA, T. OKAMOTO, M. KOIZUMI and Y. MIYAMOTO, *ibid.* **72** (1989) 1461.
4. L. S. RAMSDELL, *Amer. Min.* **32** (1947) 64.
5. P. T. B. SHAFFER, *Acta Crystallogr.* **B25** (1969) 477.
6. W. F. KNIPPENBERG, *Philips Res. Repts* **18** (1963) 161.
7. R. STEVENS, *J. Mater. Sci.* **7** (1972) 517.
8. S. SHINOZAKI and K. R. KINSMAN, *Acta Metall.* **26** (1978) 769.
9. R. S. WAGNER and W. C. ELLIS, *Trans. Met. Soc. AIME* **233** (1965) 1053.
10. I. BERMAN and C. E. RYAN, *J. Cryst. Growth* **9** (1971) 314.
11. C. E. RYAN, I. BERMAN, R. C. MARSHALL, D. P. CONSIDINE and J. J. HAWLEY, *ibid.* **1** (1967) 255.
12. P. KRISHNA and R. C. MARSHALL, *ibid.* **9** (1971) 319.
13. S. MOTOJIMA, M. HASEGAWA and H. HATTORI, *ibid.* **87** (1988) 311.
14. J. V. MILEWSKI, F. D. GAC, J. J. PETROVIC and S. R. SKAGGS, *J. Mater. Sci.* **20** (1985) 1160.
15. W. F. KNIPPENBERG and G. VERSPUI, *Mater. Res. Bull.* **4** (1969) S33.
16. K. I. PORTNOI, A. A. MUKASEEV, V. N. GRIBKOV, A. S. ISAIKIN and E. L. UMANTSEV, *Sov. Phys. Crystallogr.* **19** (1974) 198.
17. M. M. CHADWICK and T. F. MALIS, *Ultramicroscopy* **31** (1989) 205.
18. T. F. MALIS and J. M. TITCHMARSH, *Inst. Phys. Conf. Ser.* **78** (1985) 181.
19. D. W. PASHLEY and M. J. STOWELL, *Phil. Mag.* **8** (1963) 1605.
20. Y. YAN, J. CHEN, L. WANG, Q. LI, D. FENG, L. CAO and C. YAO, *Mater. Lett.* **8** (1989) 305.
21. S. R. NUTT, *J. Amer. Ceram. Soc.* **67** (1984) 428.
22. L. I. van TORNE, *J. Appl. Phys.* **37** (1966) 1849.
23. J. J. COMER, *Mater. Res. Bull.* **4** (1969) 279.
24. L. F. ALLARD, P. PENDLETON and J. S. BRINEN, in Proceedings of 44th Annual Meeting of Electron Microscopy Society of America, edited by G. W. Bailey (1986) p. 472.
25. H. IWANAGA, T. YOSHIIE, H. KATSUKI, M. EGASHIRA and S. TAKEUCHI, *J. Mater. Sci. Lett.* **5** (1986) 946.
26. H. KATSUKI, H. USHIJIMA, M. KANDA, H. IWANAGA and M. EGASHIRA, *J. Ceram. Soc. Jpn. Int. Edn* **95** (1987) 1037.
27. K. KARASEK, S. A. BRADLEY, J. T. DONNER, M. R. MARTIN, K. L. HAYNES and H. C. YEH, *J. Mater. Sci.* **24** (1989) 1617.
28. T. F. MALIS, S. C. CHENG and R. F. EGERTON, *J. Electron Micros. Techn.* **8** (1988) 193.
29. P. B. HIRSCH, A. HOWIE, R. B. NICHOLSON, D. W. PASHLEY and M. J. WHELAN, "Electron Microscopy of Thin Crystals" (Butterworths, London, 1965).
30. C. B. CARTER, *Phil. Mag. A* **50** (1984) 133.
31. J. HOMENY, W. L. VAUGHN and M. K. FERBER, *J. Amer. Ceram. Soc.* **73** (1990) 394.
32. N. W. JEPPS and T. F. PAGE, *J. Microsc.* **116** (1979) 159.
33. Y. VODAKOV, G. A. LOMAKINA, E. N. MOKHOV and V. G. ODING, *Sov. Phys. Solid State* **19** (1977) 1647.
34. Y. VODAKOV, G. LOMAKINA and E. N. MOKHOV, *ibid.* **24** (1982) 780.
35. V. A. IL'IN, M. M. PIRYUTKO, N. D. SOROKIN, Y. M. TAIROV and V. G. TSEVTKOV, *Izv. Akad. Nauk SSSR, Neorg. Mater.* **16** (1980) 1014.
36. N. D. SOROKIN, Y. M. TAIROV and V. F. TSVETKOV, *Phys. Chem. Mech. Surf.* **2** (1984) 1427.
37. S. B. AUSTERMAN and W. G. GEHMAN, *J. Mater. Sci.* **1** (1966) 249.
38. P. E. R. NORDQUIST Jr, M. L. GIPE, G. KELNER, P. H. KLEIN and R. J. GORMAN, *Mater. Lett.* **9** (1989) 17.
39. J. O. WILLIAMS and A. C. WRIGHT, *Phil. Mag. A* **55** (1987) 99.
40. G. A. BOOTSMA, W. F. KNIPPENBERG and G. VERSPUI, *J. Cryst. Growth* **11** (1971) 297.
41. J. LEE and I. B. CUTLER, *Ceram. Bull.* **54** (1975) 195.
42. B. V. SHCHETANOV, E. L. UMANTSEV, A. A. MUKASEEV and V. N. GRIBKOV, *Sov. Phys. Crystallogr.* **19** (1974) 376.
43. H. GLEITER, *Acta Metall.* **17** (1969) 1421.

Received 23 July 1990
and accepted 6 February 1991